

estimated from the rise time of the far-field waveforms from the papers used in Table 1. The thermal diffusivity for olivine is taken from C. Clauser and E. Huenges, in *A Handbook of Physical Constants: Mineral Physics and Crystallography*, T. J. Ahrens, Ed. (American Geophysical Union, Washington, DC, 1995), pp. 105–126.

23. B. V. Kostrov, *J. Appl. Math. Mech.* **30**, 1241 (1966).

24. J. D. Eshelby, *J. Mech. Phys. Solids* **17**, 177 (1969).

25. A. J. Rosakis and A. T. Zehnder, *Int. J. Fract.* **27**, 169 (1985).

26. T. Heaton, *Phys. Earth Planet. Inter.* **64**, 1 (1990).

27. Implicit in this assumption is that the frictional loss

and surface energy have the same dependence on  $V$ . If friction does not depend on  $V$ , then  $\eta$  cannot be directly related to  $V$ .

28. N. F. Mott, *Engineering* **165**, 16 (1948).

29. F. P. Bowden and T. P. Hughes, *Proc. R. Soc. London Ser. A* **172**, 280 (1939).

30. H. Houston and Q. Williams, *Nature* **352**, 520 (1991).

31. M. Furumoto, *Phys. Earth Planet. Inter.* **15**, 1 (1977).

32. D. A. Wiens and J. J. McGuire, *Geophys. Res. Lett.* **22**, 2245 (1995).

33. A. Navrotsky, in *A Handbook of Physical Constants: Mineral Physics and Crystallography*, T. J. Ahrens,

Ed. (American Geophysical Union, Washington, DC, 1995), pp. 18–28.

34. P. Lundgren and D. Giardini, *ibid.*, p. 2241.

35. S. Goes and J. Ritsema, *ibid.*, p. 2249.

36. P. F. Ihmlie and T. H. Jordan, *ibid.*, p. 2253.

37. S. L. Beck, P. Silver, T. C. Wallace, D. James, *ibid.*, p. 2257.

38. C. H. Estabrook and G. Bock, *ibid.*, p. 2277.

39. We thank J. Rice, A. Rosakis, L. Ruff, H. Houston, and A. Ruben for helpful comments.

30 September 1997; accepted 6 January 1997

## A Determination of the HDO/H<sub>2</sub>O Ratio in Comet C/1995 O1 (Hale-Bopp)

Roland Meier,\* Tobias C. Owen,\* Henry E. Matthews, David C. Jewitt,\* Dominique Bockelée-Morvan, Nicolas Biver, Jacques Crovisier, Daniel Gautier

Deuterated water (HDO) was detected in comet C/1995 O1 (Hale-Bopp) with the use of the James Clerk Maxwell Telescope on Mauna Kea, Hawaii. The inferred D/H ratio in Hale-Bopp's water is  $(3.3 \pm 0.8) \times 10^{-4}$ . This result is consistent with in situ measurements of comet P/Halley and the value found in C/1996 B2 (Hyakutake). This D/H ratio, higher than that in terrestrial water and more than 10 times the value for protosolar H<sub>2</sub>, implies that comets cannot be the only source for the oceans on Earth.

It is assumed that comets contain unprocessed matter from the earliest history of the solar system. To pursue this subject further, we measured the abundance of HDO in the coma of comet Hale-Bopp using the James Clerk Maxwell Telescope (JCMT) on Mauna Kea. The resulting D/H ratio helps define the processes leading to comet formation and trace the contribution of unmodified ice grains from the original interstellar cloud to various reservoirs of H<sub>2</sub>O throughout the solar system.

The HDO ground-state  $1_{01}-0_{00}$  transition at 464.92452 GHz was detected on 4.9 April 1997 UT (universal time) (Fig. 1), about 5 days after Hale-Bopp passed perihelion (1). At the time of the observations, the comet was 0.917 astronomical units (AU) from the sun and 1.385 AU from Earth. We used the C2 single-channel superconductor-isolator-superconductor (SIS) receiver in a double-sideband mode, which convolves the two sidebands into one spectrum. Our setup enabled simultaneous mea-

surement of two high rotational transitions in methanol (CH<sub>3</sub>OH) and the HDO line without overlap. In the upper sideband, the CH<sub>3</sub>OH  $9_2-9_1, A^\pm$  transition at 464.835 GHz and the HDO transition yielded line-integrated antenna temperatures  $\int T_A dv = 2.37 \pm 0.11$  and  $0.64 \pm 0.11$  K km s<sup>-1</sup>, respectively. The CH<sub>3</sub>OH  $11_2-11_1, A^\pm$  line at 457.006 GHz was detected in the lower sideband and had an integrated line area of  $\int T_A dv = 1.71 \pm 0.15$  K km s<sup>-1</sup> (2). At the beginning of the HDO observation, we took a SCUBA image of Hale-Bopp at 850  $\mu$ m (3). Within the typical root-mean-square mechanical stability of the telescope of  $\pm 1.5$  arc sec, this map allowed us to check our pointing. The stronger of the two CH<sub>3</sub>OH lines was then used to monitor our tracking of Hale-Bopp. To achieve continuous sky cancellation, we nodded the secondary mirror at a rate of 1 Hz with a chop throw of 180 arc sec in the azimuthal direction. During its peak-activity, Hale-Bopp was a daytime object, reaching zenith around noon. The solar elongation was 41°. JCMT is the only telescope of its class that is protected against direct solar irradiation with a membrane of woven polytetrafluoroethylene (Gore-Tex), which shades the antenna surface. The membrane transmits over 80% of the incident submillimeter radiation but reflects most of the solar light at shorter wavelengths. We obtained the HDO spectrum during a period of exceptionally dry weather. The zenith opacity at

225 GHz was  $\leq 0.06$ , which corresponds to a precipitable water column of about 1 mm.

To obtain an accurate D/H ratio in water, one would ideally want to compare HDO with an optically thin line of the rare isotopic molecules H<sub>2</sub><sup>18</sup>O or H<sub>2</sub><sup>17</sup>O using the same telescope; however, all of the stronger transitions of H<sub>2</sub><sup>18</sup>O and H<sub>2</sub><sup>17</sup>O are inaccessible to JCMT. Hence, we compared our observations with production rates measured elsewhere at about the same time. For the first week of April, a water production rate  $Q(\text{H}_2\text{O}) = (1.0 \pm 0.2) \times 10^{31} \text{ s}^{-1}$  was derived from OH observations at the Nançay radio telescope (4). An inspection of the spatial distribution of H<sub>2</sub>O (5) and ground-based OH data in the near ultraviolet (6), however, revealed that derived production rates may depend on aperture size. Follow-up measurements of HDO on 5 April indicated that the absolute calibration of the C2 receiver was not fully reliable at the time of the HDO experiment. As a check, we compared the

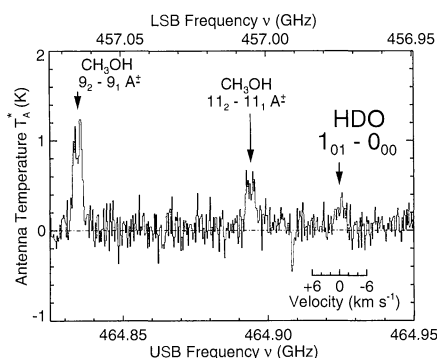


**Fig. 1.** Spectrum of Hale-Bopp showing the HDO  $1_{01}-0_{00}$  line together with two methanol transitions (120 min, on and off). The CH<sub>3</sub>OH  $11_2-11_1, A^\pm$  transition originates in the lower sideband (LSB) (top frequency scale); all other lines belong to the upper sideband (USB). Because of different calibrations of the two sidebands, the intensity of the line in the LSB has to be multiplied by a factor of 1.41 (2). Each bin covers 313 kHz and is an average of two adjacent channels. Antenna temperatures have been calibrated against internal standards and pointing sources W3(OH) and N7538 IRS1. The velocity scale for the HDO line is relative to the rest frame of the cometary nucleus. The double-peak structure of the lines is caused by the velocity distribution in the comet.

R. Meier, T. C. Owen, D. C. Jewitt, N. Biver, University of Hawaii, Institute for Astronomy, 2680 Woodlawn Drive, Honolulu, HI 96822, USA.

H. E. Matthews, Herzberg Institute for Astrophysics, National Research Council, Victoria, BC V8X 4M6, Canada, and Joint Astronomy Centre, 660 North A'Ohoku Place, Hilo, HI 96720, USA.

D. Bockelée-Morvan, J. Crovisier, D. Gautier, Observatoire de Paris-Meudon, 5 Place Jules Janssen, F-92195 Meudon, Cedex, France.

\*Visiting astronomer at the James Clerk Maxwell Telescope, 660 North A'Ohoku Place, Hilo, HI 96720, USA.

CH<sub>3</sub>OH production rate derived from the two CH<sub>3</sub>OH lines in the HDO spectrum of 4 April (Fig. 1) with those deduced from Caltech Submillimeter Observatory (CSO, Mauna Kea) and Institut de Radio Astronomie Millimétrique (IRAM, Spain) observations during the same period of time (4). Measurements at IRAM and CSO yielded  $Q(\text{CH}_3\text{OH}) = 2.3 \times 10^{29} \text{ s}^{-1}$ , a factor 1.53 higher than the value of  $1.5 \times 10^{29} \text{ s}^{-1}$  derived from the JCMT data (7). Accordingly, we adjusted the C2 temperature scale by a factor of 1.53 (8). In the millimeter and submillimeter spectral range, numerous rotational lines of CH<sub>3</sub>OH can be used to probe the gas temperature in the coma. At the time we measured HDO, the beam-averaged kinetic temperature of Hale-Bopp reached  $\sim 120 \text{ K}$  (4, 9). This temperature was measured at IRAM and CSO and is consistent with the temperature derived from the two CH<sub>3</sub>OH lines in the HDO spectrum (Fig. 1).

The D/H ratio for different excitation models and a gas temperature of 120 K were determined (Table 1). All models assumed a Gaussian beam shape with a full width at half power of  $10.3 \pm 0.5$  arc sec at 464.9 GHz. In model 1, we assumed a thermal distribution of the rotational levels at a constant equilibrium temperature. A Haser (10) model was used to describe the gas distribution in the coma. For HDO, we adopted a total photodissociation lifetime of  $7.7 \times 10^4 \text{ s}$  at 1 AU (11) and an expansion velocity of  $1.1 \text{ km s}^{-1}$ , in agreement with the line shapes. Model 1 is the simplest model and is discussed here because it is widely used and yields an upper limit and rough estimate for  $Q(\text{HDO})$ . Model 2 considers excitation of rotational levels by vi-

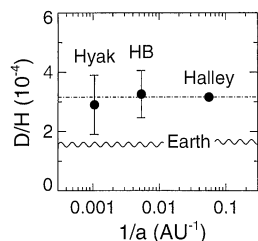


**Fig. 2.** D/H ratio of Hale-Bopp (HB), Halley (14), and Hyakutake (Hyak) (12) as a function of the (current) inverse semimajor axis  $a$ . The wavy line shows the SMOW value (15), and the dashed-dotted line, the in situ value for Halley (14). Depicted are  $1\sigma$  standard deviations. The error bar for Halley is about the size of the dot. The reciprocal semimajor axis  $1/a$  is directly related to the orbital period  $T \propto a^{2/3}$  and is a crude measure of the dynamical age of the comet. For none of the comets on our list was it possible to determine an inverse semimajor axis that is back-extrapolated in time,  $(1/a)_0$ , a quantity which would have provided a more realistic measure for the dynamical age (16).

brational levels in the infrared and by collisions with neutral water molecules (12). Unlike in model 1, no equilibrium is assumed. Instead, the model accounts for the changing physical environment as the coma expands radially outward. In the first few thousand kilometers from the nucleus, collisions determine the population of the rotational levels, and at larger distances, radiative processes prevail. Model 2 depends on the number of collision partners given by  $Q(\text{H}_2\text{O}) = 1 \times 10^{31} \text{ s}^{-1}$  and on the adopted collision cross section  $\sigma_{\text{coll}} = 5 \times 10^{-14} \text{ cm}^2$ . Model 3 is an improved version of model 2 that includes collisions with electrons (13). The effects of optical depth are negligible for HDO. The more elaborate models 2 and 3 are less sensitive to the gas temperature than model 1 because a sizable fraction of the total line flux originates from areas in the beam where fluorescence excitation dominates over collisional excitation. Model 3 with the preferred temperature gives an HDO production rate of  $Q(\text{HDO}) = (6.5 \pm 1.1) \times 10^{27} \text{ s}^{-1}$  or a D/H ratio in water of  $(\text{D}/\text{H})_{\text{H}_2\text{O}} = (3.3 \pm 0.8) \times 10^{-4}$ . The  $1\sigma$  error for  $(\text{D}/\text{H})_{\text{H}_2\text{O}}$  is the sum of the formal errors of  $Q(\text{HDO})$  and  $Q(\text{H}_2\text{O})$ .

We now have three values of D/H in cometary H<sub>2</sub>O (Fig. 2). Of these, only the Halley value was an in situ measurement; hence, its precision is correspondingly greater (14). Nevertheless, it appears that the  $(\text{D}/\text{H})_{\text{H}_2\text{O}}$  values in these three comets are similar to each other and higher than the value for standard mean ocean water (SMOW), which is  $(\text{D}/\text{H})_{\text{H}_2\text{O}} = 1.56 \times 10^{-4}$  (15). Although the three comets vary in their gas-to-dust ratio, size, and orbital period, the retrograde orbit of Halley and the long orbital periods and high inclinations of Hyakutake and Hale-Bopp (16) suggest that the Oort cloud is the source region for all three. It seems for the moment reasonable to accept the Halley value as characteristic of ices in Oort cloud comets, on the basis of this sample. Note that we do not yet have a value of

D/H in a Jupiter family comet, that is, a short-period comet that is in a low-inclination direct orbit, indicating an origin in the Kuiper Belt (17). As all three of the comets appear to have come from the Oort cloud, statistics favor their origin in the Uranus-Neptune region of the solar nebula (18).

The relatively high cometary  $(\text{D}/\text{H})_{\text{H}_2\text{O}}$  ratio helps us understand processes in the primordial nebula. Evidently, radial mixing was not very thorough because the mixture of ices that formed Earth's oceans is not the same as the mixture we find in the comets (14). We find high  $(\text{D}/\text{H})_{\text{H}_2\text{O}}$  values ( $1 \times 10^{-4}$  to  $5 \times 10^{-4}$ ) in the cores of hot ( $\sim 200 \text{ K}$ ) interstellar clouds (19). In hot cores, the high values of  $\text{HDO}/\text{H}_2\text{O}$  may reflect the composition of icy grain mantles that formed in an earlier cold phase (19). Millar *et al.* (20) have calculated that a steady-state value of  $6.4 \times 10^{-4}$  for  $\text{HDO}/\text{H}_2\text{O}$  will be achieved in an interstellar cloud at a temperature of about  $35 \pm 10 \text{ K}$  as a result of gas-phase ion-molecule reactions. Brown and Millar (21) have shown that still higher values of D/H could occur as a result of interactions with grain surfaces. The absence of ionization and the low ambient temperature ( $50 \pm 20 \text{ K}$ ) in the Uranus-Neptune region of the solar nebula, the source region for Oort-cloud comets, ensure that little change in the interstellar medium values of D/H will occur during comet formation even if the icy grain mantles sublimate as the particles fall into the solar nebula mid-plane, to recondense on their refractory cores at the local temperature of the nebula (22). Our  $(\text{D}/\text{H})_{\text{H}_2\text{O}}$  measurement therefore strengthens the case for the primitive nature of cometary material. It invites further study of D/H in other H-bearing species in comets, as experience with interstellar clouds dictates that these values will not be the same as  $(\text{D}/\text{H})_{\text{H}_2\text{O}}$  in SMOW (23). Although we must still await determinations of HDO in classical short period comets to be certain, it appears that comets by themselves cannot be the only

**Table 1.** D/H of water in Hale-Bopp.  $T_{\text{gas}}$  is the kinetic gas temperature (results for 80 K are shown to illustrate the temperature dependence);  $\int T_{\text{B}} dv$  is the calculated main beam efficiency-corrected line area for  $Q(\text{HDO}) = 1.0 \times 10^{27} \text{ s}^{-1}$ ;  $\langle N \rangle$  is the beam-averaged column density for the measured value  $\int T_{\text{B}} dv = 1.85 \text{ K km s}^{-1}$  (2); and  $Q(\text{HDO})$  is the nuclear production rate of HDO. Note that  $(\text{D}/\text{H})_{\text{H}_2\text{O}} = 0.5[Q(\text{HDO})/Q(\text{H}_2\text{O})]$ .

Model	$T_{\text{gas}}$ (K)	$\int T_{\text{B}} dv$ (K km s <sup>-1</sup> )	$\langle N \rangle$ (cm <sup>-2</sup> )	$Q(\text{HDO})$ (s <sup>-1</sup> )	$(\text{D}/\text{H})_{\text{H}_2\text{O}}$
1	80	0.26	$4.2 \times 10^{13}$	$7.1 \times 10^{27}$	$3.5 \times 10^{-4}$
	120	0.16	$6.9 \times 10^{13}$	$11.7 \times 10^{27}$	$5.9 \times 10^{-4}$
2	80	0.42	$2.6 \times 10^{13}$	$4.4 \times 10^{27}$	$2.2 \times 10^{-4}$
	120	0.31	$3.6 \times 10^{13}$	$6.1 \times 10^{27}$	$3.0 \times 10^{-4}$
3	80	0.40	$2.8 \times 10^{13}$	$4.7 \times 10^{27}$	$2.4 \times 10^{-4}$
	120	0.28	$3.9 \times 10^{13}$	$6.5 \times 10^{27}$	$3.3 \times 10^{-4}$

source of water for Earth's oceans (14). This result was anticipated from the high value of O/C in Earth's crust (24), but D/H provides a much stronger argument (14). Mixing of cometary water with water absorbed from the solar nebula by the rocky grains that accreted to form Earth may provide the observed value of (D/H)<sub>SMOW</sub> (25), as water vapor in the inner solar nebula could have D/H < 1 × 10<sup>-4</sup> (26).

## REFERENCES AND NOTES

1. R. Meier *et al.*, *IAU Circ.* 6615 (1997).
2. Line areas are integrated over a velocity interval of ±3 km s<sup>-1</sup>. Sky noise is the dominant source for the statistical uncertainties of the lines. The ratio of the system temperature in the image and signal sideband was  $f = 1.41$ . Because the system cannot distinguish between the two sidebands, it scales all lines according to the calibrated upper sideband, which means that the line area of CH<sub>3</sub>OH 11<sub>2</sub>-11<sub>1</sub> A<sup>±</sup> in the lower sideband has to be multiplied by  $f$ . To obtain main beam corrected and absolutely calibrated line areas, the measured antenna temperature has to be divided by the main beam efficiency  $\eta = 0.53 \pm 0.05$  and re-scaled by a factor of 1.53 (see text).
3. At 850  $\mu\text{m}$ , the submillimeter common-user bolometer array (SCUBA) of JCMT uses an array of 37 pixels cooled to around 100 mK.
4. N. Biver *et al.*, *Bull. Am. Astron. Soc.* 29, 1047 (1997).
5. N. Dello Russo *et al.*, *ibid.*, p. 1050.
6. D. G. Schleicher, R. L. Millis, T. L. Farnham, S. M. Lederer, *ibid.*, p. 1033.
7. To obtain consistent production rates  $Q(\text{CH}_3\text{OH})$ , we applied the same model and model parameters to the various measurements. From CSO and IRAM data recorded at the time of the HDO observations, a ratio  $Q(\text{CH}_3\text{OH})/Q(\text{H}_2\text{O})$  was derived that agreed with ratios measured with the same telescopes on various occasions in March and April 1997 (4). This fact suggests that the JCMT observations were affected by calibration or pointing problems, although time variability in the cometary activity cannot be excluded.
8. This adjustment is equivalent to the statement that for the purpose of deriving a D/H ratio in water, we compare the  $Q(\text{HDO})/Q(\text{CH}_3\text{OH})$  ratio with the  $Q(\text{CH}_3\text{OH})/Q(\text{H}_2\text{O})$  ratio derived from CSO and IRAM measurements during March and April. The  $Q(\text{HDO})/Q(\text{CH}_3\text{OH})$  ratio does not depend on an absolute calibration. Ratios are only slightly affected by aperture effects, pointing, and comet variability, especially because CH<sub>3</sub>OH and H<sub>2</sub>O are long-lived species with comparable lifetimes against photodissociation.
9. D. Mehringer *et al.*, *IAU Circ.* 6614 (1997).
10. L. Haser, *Acad. R. Sci. Liege* 43, 740 (1957).
11. J. Crovisier, *J. Geophys. Res.* 99, 3777 (1994).
12. D. Bockelée-Morvan *et al.*, in preparation.
13. N. Biver, thesis, Université Paris VII (1997).
14. P. Eberhardt, M. Reber, D. Krankowsky, R. R. Hodges, *Astron. Astrophys.* 302, 301 (1995); H. Balsiger, K. Altwegg, J. Geiss, *J. Geophys. Res.* 100, 5827 (1995).
15. R. Hagemann, G. Nief, E. Roth, *Tellus* 22, 712 (1970); J. P. De Witt, C. M. Van der Straaten, W. G. Mook, *Geostand. Newsl.* 4, 33 (1980).
16. For example, M. E. Bailey *et al.* [*Mon. Not. R. Astron. Soc.* 281, 916 (1996)] conducted extensive numerical simulations on the orbital evolution of Hale-Bopp.
17. H. F. Levison and M. J. Duncan, *Icarus* 108, 18 (1994).
18. J. H. Oort, *Bull. Astron. Inst. Neth.* 11, 91 (1950); P. R. Weissman, in *Comets in the Post-Halley Era*, R. L. Newburn *et al.*, Eds. (Kluwer Academic, Dordrecht, Netherlands, 1991), vol. 1, pp. 463–486.
19. R. D. Gensheimer, R. Mauersberger, T. L. Wilson, *Astron. Astrophys.* 314, 281 (1996).

20. T. J. Millar, A. Bennett, E. Herbst, *Astrophys. J.* 340, 906 (1989).
21. P. D. Brown and T. J. Miller, *Mon. Not. R. Astron. Soc.* 237, 661 (1989).
22. J. L. Lunine, S. Engel, B. Risz, M. Horanyi, *Icarus* 94, 333 (1991).
23. W. M. Irvine and R. F. Knacke, in *Origin and Evolution of Planetary and Satellite Atmospheres*, S. K. Atreya, J. B. Pollack, M. S. Matthews, Eds. (Univ. of Arizona Press, Tucson, 1989), pp. 3–34.
24. T. C. Owen and A. Bar-Nun, *Icarus* 116, 215 (1995).
25. T. Owen, in *From Stardust to Planetesimals*, Y. J. Pendleton and A. G. G. M. Tielens, Eds. (ASP Publ. 122, Astronomical Society of the Pacific, San Francisco, 1997), pp. 435–450.
26. C. Lecluse and F. Robert, *Geochim. Cosmochim. Acta* 58, 2927 (1994).

27. We thank M. Mumma and N. Dello Russo for providing us with H<sub>2</sub>O production rates before publication, D. G. Schleicher for helpful discussion of his prepublication OH observations, the operators of JCMT for their assistance, P. Eberhardt for valuable comments on the manuscript, and B. Marsden and D. Tholen for help with the ephemerides. This work was supported by NASA grants NAEW 2650 and NAEW 2631. D.C.J. acknowledges support from NSF grant AST96-15603. The JCMT is operated by the Joint Astronomy Centre on behalf of the Particle Physics and Astronomy Research Council of the United Kingdom, the Netherlands Organisation for Scientific Research, and the National Research Council of Canada.

2 October 1997; accepted 29 December 1997

## Water in Betelgeuse and Antares

Donald E. Jennings\*† and Pedro V. Sada\*

Absorption lines of hot water have been identified in the infrared spectra of Betelgeuse ( $\alpha$  Orionis) and Antares ( $\alpha$  Scorpii) near 12.3 micrometers (811 to 819 wavenumbers). The water lines originate in the atmospheres of the stars, not in their circumstellar material. The spectra are similar in structure to umbral sunspot spectra. Pure rotation water lines of this type will occur throughout the spectra of cool stars at wavelengths greater than 10 micrometers. From the water spectra, the upper limit for the temperature in the line formation region in both stars is 2800 kelvin. The water column density in both stars is  $(3 \pm 2) \times 10^{18}$  molecules per square centimeter, yielding an abundance relative to atomic hydrogen of  $n(\text{H}_2\text{O})/n(\text{H}) \approx 10^{-7}$ .

Water is abundant in cool stars (1) and is a major molecular constituent at low temperatures in oxygen-rich stars, dominating all molecules other than CO and H<sub>2</sub> in regions at temperatures below 2000 K (2). The spectrum of hot water is most commonly observed in the near infrared at wavelengths between 0.9 and 3.2  $\mu\text{m}$  (3–5). In M-type stars, strong H<sub>2</sub>O absorption is seen in Mira-type variables, whereas non-variable stars have weaker or no water absorption [see (3), for example]. Recently, water was detected in sunspots (6), where the temperature can be as low as in M-type stars. Water dominates the spectrum in sunspots at 10 to 20  $\mu\text{m}$ , as identified from laboratory studies of water spectra taken at high temperatures (6–8). At 3000 to 4000 K, sunspots provide a starting point in a search for hot water in stars cooler than the sun, even though the physical conditions other than temperature are different. The improved understanding of sunspot spectra, plus the laboratory and theoretical characterization of the pure-rotation region of hot

water, motivated us to obtain spectra of M-type supergiants.

Betelgeuse [ $\alpha$  Orionis ( $\alpha$  Ori, class M1-2 Ia-Iab)] and Antares [ $\alpha$  Scorpii ( $\alpha$  Sco, M1.5 Iab-Ib)] are among the brightest late M-type supergiants. They are both oxygen-rich with visible effective temperatures near 3500 K (9). They also both exhibit the extended atmospheres typical of red supergiants and have circumstellar dust shells with inner radii of more than 25 stellar radii (10) and mass loss rates of 10<sup>-6</sup> to 10<sup>-5</sup> solar masses per year (11). Both undergo irregular or semiregular variability.

Betelgeuse ( $\alpha$  Ori) is the brightest and most studied M-type supergiant. The continuum flux from this star at 12  $\mu\text{m}$  is a combination of radiation from the chromosphere at about 3200 K (12) and a circumstellar dust shell at about 500 K (13). The star's magnitude at 12  $\mu\text{m}$  is -5.5 (14); it is a semiregular variable with a recent visual luminosity range between magnitudes 0.3 and 0.9 and a period of about 6 years (12). It changes by 0.1 magnitude at 11  $\mu\text{m}$  during a period (12). Both CO and SiO are observed in the circumstellar envelope (15), but water was not reported in spectra of this star (16), and it has been used as a water-free reference source (4).

Antares ( $\alpha$  Sco) has a binary companion, a fainter dwarf B-type star with a separation of 2.9 arc sec. The visual magni-

D. E. Jennings, Planetary Systems Branch, Code 693, NASA Goddard Space Flight Center, Greenbelt, MD 20771, USA.

P. V. Sada, Consultoría Astronómica de Monterrey, Bosques de Pirineos 520-3, Col. Bosques del Valle, Garza García, N.L. 66250, México.

\*Visiting Astronomer, National Solar Observatory, Tucson, AZ 85726, USA.

†To whom correspondence should be addressed.